

# LoCo: Locally Constrained Training-Free Layout-to-Image Synthesis

Peiang Zhao<sup>1</sup> Han Li<sup>1</sup> Ruiyang Jin<sup>1</sup> S. Kevin Zhou<sup>1,2</sup>

<sup>1</sup> Center for Medical Imaging, Robotics, Analytic Computing & Learning (MIRACLE), Suzhou Institute for Advanced Research, University of Science and Technology of China

<sup>2</sup> Key Lab of Intelligent Information Processing of Chinese Academy of Sciences (CAS), Institute of Computing Technology

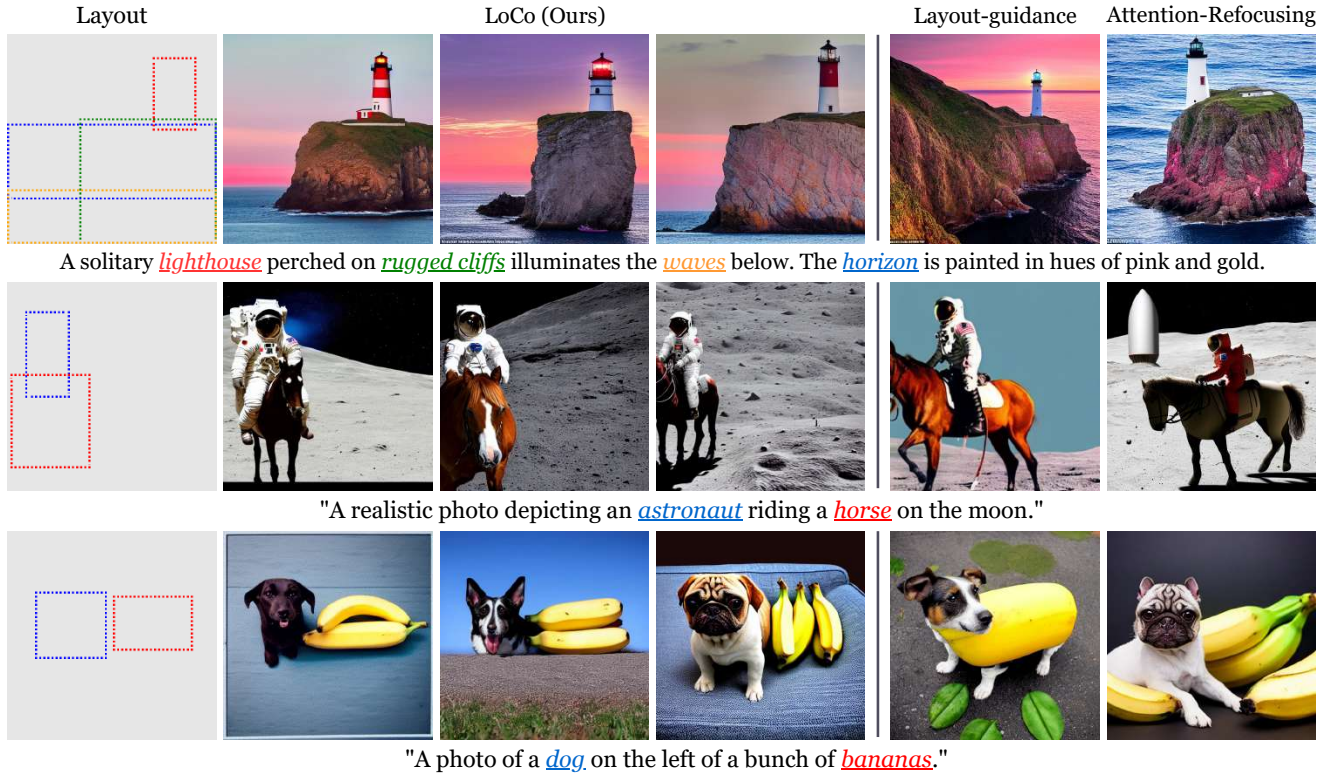


Figure 1. Existing training-free layout-to-image synthesis approaches struggle to generate high-quality images that adhere to the given textual prompts and spatial layout. In contrast, LoCo is able to handle various spatial layouts and unusual prompts while maintaining high image quality and precise concept coverage.

## Abstract

Recent text-to-image diffusion models have reached an unprecedented level in generating high-quality images. However, their exclusive reliance on textual prompts often falls short in accurately conveying fine-grained spatial compositions. In this paper, we propose LoCo, a training-free approach for layout-to-image synthesis that excels in producing high-quality images aligned with both textual prompts and spatial layouts. Our method introduces a Lo-

calized Attention Constraint to refine cross-attention for individual objects, ensuring their precise placement in designated regions. We further propose a Padding Token Constraint to leverage the semantic information embedded in previously neglected padding tokens, thereby preventing the undesired fusion of synthesized objects. LoCo seamlessly integrates into existing text-to-image and layout-to-image models, significantly amplifying their performance and effectively addressing semantic failures observed in prior methods. Through extensive experiments, we showcase the

superiority of our approach, surpassing existing state-of-the-art training-free layout-to-image methods both qualitatively and quantitatively across multiple benchmarks.

## 1. Introduction

Recently, text-to-image diffusion models such as DALL-E 2 [24], Imagen [28], and Stable Diffusion [26], have demonstrated an unprecedented capacity for synthesizing high-quality images conditioned on textual input. This advancement has garnered a significant attention from both the research community and the general public, leading to a rise of numerous image editing tools and simplifying the process of creative media design.

Despite these successes, a significant challenge faced by these models is that they rely solely on textual prompts for spatial composition control, which is inadequate for many applications. For instance, in movie poster design, where both content and layout are pivotal, dependence solely on text may prove insufficient. While texts can harness a rich repository of high-level concepts, they struggle to convey the fine-grained spatial composition of an image accurately. Utilizing position-related descriptions like “on the left” and “beneath” can only provide limited spatial control, often resulting in ambiguous images. The challenge intensifies when the description becomes complex or involves an unusual scene.

To tackle this challenge, layout-to-image synthesis (LIS) [1, 7, 10, 16, 17, 30, 32, 38–40] has been studied to synthesize images adhering to the spatial layout input. Fully supervised LIS methods have demonstrated impressive results. While SceneComposer [38] trains entirely new layout-to-image models, other approaches such as GLIGEN [16] and ControlNet [39] enhance existing models with additional modules. Unfortunately, these approaches demand considerable amounts of paired layout-image training data, which are costly and challenging to acquire. Moreover, both training and fine-tuning a model are computationally intensive.

On the contrary, a noteworthy line of research [6, 8, 11, 15, 21, 34] demonstrates that layout-to-image synthesis can be achieved in a training-free manner. Specifically, these methods guide the synthesis process by manipulating cross-attention maps based on the input layout. However, these methods suffer from semantic inconsistency issues, which originate from the original text-to-image models (e.g., Stable Diffusion [26]). For instance, two typical types of semantic failures in state-of-the-art training-free LIS approaches are illustrated in Fig. 2: (1) “Object Fusion”, where two or more desired objects are incorrectly merged, particularly when they are closely located, and (2) “Semantic Neglect”, where some desired objects in the user-provided prompt are not generated at all.

In this paper, we introduce **LoCo**, short for Locally

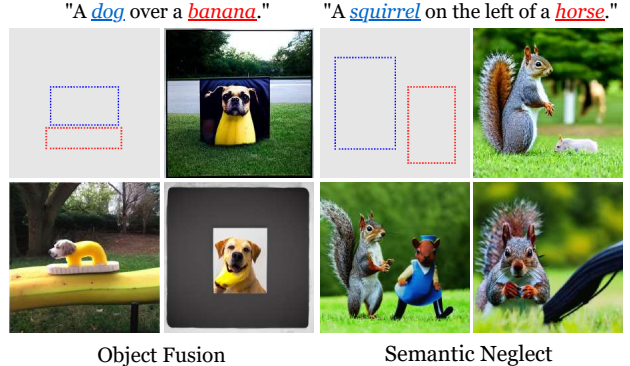


Figure 2. Typical semantic failures in layout-to-image synthesis (LIS). Even the state-of-the-art training-free LIS methods produce unsatisfactory images when dealing with simple conditions.

Constrained Diffusion, an novel training-free approach designed to enhance positional accuracy in layout-to-image synthesis and address semantic failures. Specifically, we enhance the latent feature update (or denoising) step in the diffusion process by integrating two novel constraints, the **Localized Attention Constraint** ( $\mathcal{L}_{LAC}$ ) and the **Padding Tokens Constraint** ( $\mathcal{L}_{PTC}$ ), based on the cross-attention maps extracted at each denoising timestep.

The  $\mathcal{L}_{LAC}$  aims to ensure accurate generation of desired objects. Diverging from existing methods,  $\mathcal{L}_{LAC}$  refines the guidance strength with cross-attention maps normalization, allowing for more precise and moderate latent feature manipulation. This fine-tuning effectively avoids image quality deterioration caused by excessive guidance, addressing the issue of semantic neglect.  $\mathcal{L}_{PTC}$  taps into previously overlooked semantic information carried by padding tokens, specifically start-of-text tokens ( $[SOT]$ ) and end-of-text tokens ( $[EOT]$ ) in textual embedding. These tokens hold significant associations with the layout of the synthesized image. By leveraging this information,  $\mathcal{L}_{PTC}$  prevents closely-located objects from extending beyond their designated boxes, thereby efficiently averting the incorrect fusion of desired objects.

We conduct comprehensive experiments, comparing our method with various approaches in the layout-to-image synthesis literature. Our results demonstrate state-of-the-art performances, showcasing improvements both quantitatively and qualitatively over prior approaches.

In summary, our contributions are as follows:

- We introduce LoCo, a training-free method for layout-to-image synthesis that excels in producing high-quality images aligned with both textual prompts and spatial layouts.
- We present  $\mathcal{L}_{LAC}$  and  $\mathcal{L}_{PTC}$  to address semantic failures while ensuring layout control effects. The former serves as an effective constraint, mitigating semantic ne-

glect without compromising image quality. The latter leverages the semantic information embedded in previously neglected padding tokens, preventing the undesired blending of synthesized objects.

- We conduct comprehensive experiments, comparing our approach with existing models in the layout-to-image synthesis literature. The results showcase that LoCo outperforms prior state-of-the-art approaches, considering both quantitative metrics and qualitative assessments.

## 2. Related Work

### 2.1. Text-to-Image Diffusion models

Large-scale text-to-image diffusion models have garnered substantial attention due to their remarkable performances. For instance, Ramesh *et al.* [24] introduce the pre-trained CLIP [23] model to text-to-image generation, demonstrating its efficacy in aligning images and text features. Rombach *et al.* [26] propose LDM, leveraging a powerful autoencoder to streamline the computational load of the iterative denoising process. These pioneering efforts directly contribute to the inception of Stable Diffusion, elevating text-to-image generation to unprecedented levels of prominence within both the research community and the general public. Subsequent studies [3, 9, 14, 25, 31] aim to improve the performance further. Notably, SD-XL [22] employs a larger backbone and incorporates diverse conditioning mechanisms, resulting in its ability to generate photorealistic high-resolution images. However, a notable limitation persists across these methods — they heavily rely on textual prompts as conditions, thus impeding precise control over the spatial composition of the generated image.

### 2.2. Layout-to-Image Synthesis

Layout-to-image synthesis (LIS) revolves around generating images that conform to specified bounding boxes or semantic masks of object categories. Several approaches [1, 16, 19, 33, 35–39] suggest using paired layout-image data for training new models or fine-tuning existing ones. For example, SceneComposer [38] trains a layout-to-image model using a paired dataset of images and segmentation maps. In parallel, ControlNet [39] and GLIGEN [16] employ effective fine-tuning methods, integrating additional components or adapters. While these methods yield noteworthy results, they grapple with the challenge of labor-intensive and time-consuming data collection for training. Furthermore, a fully-supervised pipeline entails additional computational resource consumption and prolonged inference times.

Another series of methods [6, 8, 11, 15, 21, 34] address the issue through a training-free approach with pre-trained models. Hertz *et al.* [12] initially observe that the spatial layouts of generated images are intrinsically con-

nected with cross-attention maps. Building on this insight, Directed Diffusion[20] and DenseDiffusion [15] lead the way in manipulating the cross-attention map to align generated images with layouts. Subsequently, BoxNet [33] acts on cross-attention maps with an object box prediction module, estimating object locations at any timestep during the forward diffusion process. Numerous concurrent studies also propose various methods for modulating cross-attention maps. Regrettably, even the state-of-the-art training-free approaches encounter semantic failures when interpreting simple layout instructions.

Closer to our work, BoxDiff [34] encourages the desired objects to appear in the specified region by calculating losses based on the maximum values in cross-attention maps. Similarly, Attention-Refocusing [21] modifies both cross-attention and self-attention maps to control object positions. Through our experiments, we observe that these approaches may overly strengthen the guidance, resulting in semantic neglect and image quality degradation. Therefore, we introduce  $\mathcal{L}_{LAC}$  to ensure a moderate guidance while ensuring control effects. Chen *et al.* [6] notice a counter-intuitive phenomenon that padding tokens, *i.e.*, start-of-text tokens ( $[SOT]$ ) and end-of-text tokens ( $[EOT]$ ), inherently carry rich semantic and layout information. However, this observation has not been thoroughly explored and utilized. Our  $\mathcal{L}_{PTC}$  efficiently harnesses the information embedded in padding tokens to avoid the undesired fusion of generated objects.

## 3. Method

In this section, we discuss our method for layout-to-image synthesis. We begin with a concise overview of the cross-attention mechanism and the problem setup, followed by a detailed presentation of the key components of LoCo.

### 3.1. Preliminaries

**Attention map extraction.** The Stable Diffusion model utilizes a cross-modal attention between text tokens and latent features to condition the image synthesis. Given a text prompt  $\mathbf{y}$ , a pre-trained CLIP [23] encoder is used to get the text tokens  $\mathbf{e} = f_{\text{CLIP}}(\mathbf{y}) \in \mathbb{R}^{n \times d_e}$ , *i.e.*, text embedding features. The *query*  $\mathbf{Q} \in \mathbb{R}^{q \times d}$  and *value*  $\mathbf{K} \in \mathbb{R}^{n \times d}$  are the projection of latent features  $\mathbf{z}_t$  and text tokens  $\mathbf{e}$ , respectively. In the denoising step, the cross-attention  $\mathbf{A}$  can be acquired as follows:

$$\mathbf{A} = \text{Softmax} \left( \frac{\mathbf{Q}\mathbf{K}^\top}{\sqrt{d}} \right) \in [0, 1]^{q \times n} \quad (1)$$

in which  $q = h \times w$ , denoting the spatial resolutions of the cross-attention  $\mathbf{A}$ . At each timestep  $t$ , we can obtain a set of cross-attention maps  $\mathbf{A}^t = \{\mathbf{A}_0^t, \dots, \mathbf{A}_{n-1}^t\}$  containing  $n$  spatial attention maps, where  $\mathbf{A}_i^t$  corresponds to the  $i$ -th text token  $\mathbf{e}_i$ .



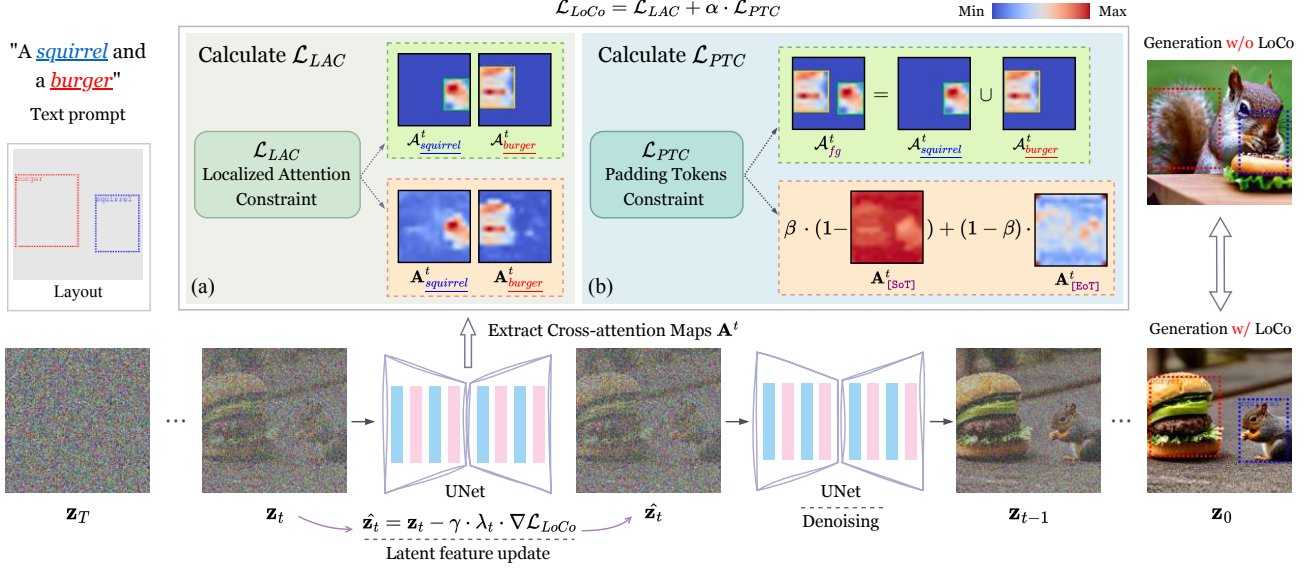


Figure 3. **Overview of LoCo.** At timestep  $t$ , we pass current latent feature  $\mathbf{z}_t$  through the UNet [27] to extract the cross-attention maps  $\mathbf{A}^t$ . Given the textual prompt and box conditions, we obtain target map  $\mathcal{A}_i^t$  for the cross-attention map  $\mathbf{A}_i^t$  associated with the  $i$ -th desired object. Here, we use  $\mathbf{A}_{object}^t$  (e.g.  $\mathbf{A}_{squirrel}^t$ ) to denote  $\mathbf{A}_i^t$  for clarity. The proposed constraints, i.e.,  $\mathcal{L}_{LAC}$  and  $\mathcal{L}_{PTC}$ , are then applied. Consequently, the current latent feature  $\mathbf{z}_t$  is updated with the  $\nabla \mathcal{L}_{LoCo}$  to obtain  $\hat{\mathbf{z}}_t$  for denoising.

Please note that, unlike previous methods, we preserve cross-attention maps of the start-of-text token (i.e., [SoT]) and the end-of-text token (i.e., [EoT]). Similar to [8], our proposed constraints are applied on the cross-attentions with a resolution of  $16 \times 16$  to achieve the optimal trade-off between image quality and layout control.

**Problem setup.** We consider the input layout as  $k$  bounding boxes  $\mathcal{B} = \{\mathbf{b}_1, \dots, \mathbf{b}_k\}$  and  $k$  corresponding textual phrases  $\mathcal{W} = \{\mathbf{w}_1, \dots, \mathbf{w}_k\}$ , with  $\mathbf{b}_i$  indicating the user-provide location for each object and  $\mathbf{w}_i$  describing the desired object in detail. Before applying the proposed constraints, we transform and resize each bounding box  $\mathbf{b}_i$  to its corresponding binary mask  $\mathbf{M}_i$  where  $\mathbf{M}_i \in \mathbb{R}^{16 \times 16}$ .

### 3.2. Localized Attention Constraint (LAC)

As demonstrated in prior studies [12, 15, 34], during the denoising step of the Stable Diffusion model, the location and scale of high-response regions in the cross-attention map perceptually align with those of synthesized objects in the decoded image. Hence, to encourage the  $i$ -th desired object to appear at the specified location, we compare its corresponding cross-attention map  $\mathbf{A}_i^t$  with the target map  $\mathcal{A}_i^t$  with Localized Attention Constraint  $\mathcal{L}_{LAC}$  (Fig. 3 (a)). We obtain  $\mathcal{A}_i^t$  as follows:

$$\mathcal{A}_i^t = \mathbf{A}_i^t \odot \mathbf{M}_i \quad (2)$$

and the  $\mathcal{L}_{LAC}$  writes:

$$\mathcal{L}_{LAC} = \left[ 1 - \frac{\sum_{w_i \in \mathcal{W}} \text{sum}(\frac{\mathbf{A}_i^t}{\|\mathbf{A}_i^t\|_\infty})}{\sum_{w_i \in \mathcal{W}} \text{sum}(\frac{\mathbf{A}_i^t}{\|\mathbf{A}_i^t\|_\infty})} \right]^2 \quad (3)$$

where  $\text{sum}(\cdot)$  means that we calculate the accumulation of each pixel value in the cross-attention map.

Please note that we normalize each original cross-attention map  $\mathbf{A}_i^t$  individually with  $\|\mathbf{A}_i^t\|_\infty$ . This operation is motivated by a crucial observation. Specifically, while the high-response regions in the cross-attention map are perceptually equivalent to the positions of synthesized objects in the image, the maxima of these regions are numerically small (around 0.1). Therefore, constraints in the form of “ $1 - \max(\mathbf{A}_i^t)$ ” as in previous arts would lead to over-guidance and, consequently, semantic neglect. Normalization makes  $\mathbf{A}_i^t$  more comparable to the optimization target  $\mathcal{A}_i^t$ , facilitating a moderate guidance and preventing semantic neglect while ensuring control effects.

### 3.3. Padding Tokens Constraint (PTC)

The involvement of  $\mathcal{L}_{LAC}$  only refocuses the cross-attention to attend the correct regions. However, when these specified regions are located close together, the synthesized objects sometimes go beyond the bounding box and blend incorrectly.

Building upon the insights from Chen *et al.* [6], we introduce  $\mathcal{L}_{PTC}$  (Fig. 3 (b)), which leverages the rich semantic and layout information in padding tokens to prevent object

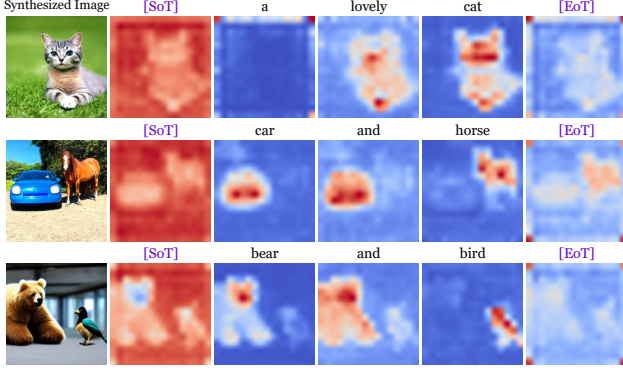


Figure 4. Visualization of cross-attention maps between different text tokens and the intermediate image latent feature. One can observe from the examples that the padding tokens, *i.e.*, start-of-text tokens ( $[SoT]$ ) and end-of-text tokens ( $[EoT]$ ) also carry substantial semantic and layout information.

fusion. Initially, we derive the target map  $\mathcal{A}_{fg}^t$  for all foreground objects :

$$\mathcal{A}_{fg}^t = \bigcup_{i=1}^n \mathcal{A}_i^t \quad (4)$$

As illustrated in Fig. 4, both  $[SoT]$  and  $[EoT]$  tokens contain information about the image layout. While  $[SoT]$  primarily emphasizes the background,  $[EoT]$  responds to the foreground complementarily. Hence, we propose calculating  $\mathbf{A}_{PT}^t$  as follows:

$$\mathbf{A}_{PT}^t = \beta \cdot \frac{1 - \mathbf{A}_{SoT}^t}{\|1 - \mathbf{A}_{SoT}^t\|_\infty} + (1 - \beta) \frac{\mathbf{A}_{EoT}^t}{\|\mathbf{A}_{EoT}^t\|_\infty} \quad (5)$$

in which  $\beta$  serves as a weighting factor and  $\mathbf{A}_{PT}^t$  is a weighted average of the reversion of normalized  $\mathbf{A}_{SoT}^t$  and normalized  $\mathbf{A}_{EoT}^t$ . Subsequently, we propose the Padding Tokens Constraint  $\mathcal{L}_{PTC}$  as below:

$$\mathcal{L}_{PTC} = \mathcal{L}_{BCE} [\text{Sigmoid}(\mathbf{A}_{PT}^t), \mathbf{A}_{PT}^t] \quad (6)$$

where  $\mathcal{L}_{BCE}$  represents the binary cross-entropy loss. Here,  $\mathcal{L}_{PTC}$  aims to minimize cross-attention responses outside the target regions, effectively preventing the incorrect fusion of desired objects when their designated locations are in close proximity.

### 3.4. Latent Feature Update

At each timestep  $t$ , the overall constraint  $\mathcal{L}_{LoCo}$  is the weighted summation of  $\mathcal{L}_{LAC}$  and  $\mathcal{L}_{PTC}$  as follows:

$$\mathcal{L}_{LoCo} = \mathcal{L}_{LAC} + \alpha \cdot \mathcal{L}_{PTC} \quad (7)$$

Here,  $\alpha$  is a factor controlling the intervention strength of  $\mathcal{L}_{PTC}$ . We update the current latent feature  $\mathbf{z}_t$  via back-propagation with  $\mathcal{L}$  as below:

$$\hat{\mathbf{z}}_t \leftarrow \mathbf{z}_t - \gamma \cdot \lambda_t \cdot \nabla \mathcal{L}_{LoCo} \quad (8)$$

Here,  $\gamma$  is a scale factor controlling the strength of the guidance, and  $\lambda_t$  represents the noise schedule, decaying at each timestep. Subsequently,  $\hat{\mathbf{z}}_t$  is sent for denoising.

Guided by  $\mathcal{L}_{LoCo}$ ,  $\mathbf{z}_t$  gradually adjusts at each timestep, aligning high-response attention regions to the specified bounding boxes. This process leads to the synthesis of target objects in the user-provided locations. Please refer to the experimental section for additional details.

## 4. Experiments

### 4.1. Experimental Setup

**Datasets.** We conduct experiments on two standard benchmarks for text-to-image models, the **HRS-Bench** [2] and the **DrawBench** [28]. The HRS-Bench serves as a comprehensive benchmark for text-to-image models, offering various prompts divided into three main topics: accuracy, robustness, and generalization. As our method focuses on layout control, we specifically select three categories from HRS: *spatial relationship*, *size*, and *color*. The number of prompts for each category is 1002/501/501, respectively. The DrawBench dataset is a challenging benchmark for fine-grained analysis of text-to-image models. For evaluation, we utilize the category of *Positional* in DrawBench. Since both HRS and DrawBench do not include layout conditions, we incorporate publicly available layout labels published by Phung et al. [21] for evaluation. To further assess the performance of selected methods in generating photo-realistic images, we curate a COCO subset by randomly selecting 100 samples, along with their corresponding captions and bounding boxes from the **MS-COCO** [18] dataset.

**Evaluation Metrics.** We follow the standard evaluation protocol of HRS. Specifically, we employ the pre-trained UniDet [41], a multi-dataset detector, on all synthesized images. Predicted bounding boxes are then utilized to validate whether the spatial relation is grounded correctly. For the chosen categories, **generation accuracy** serves as the evaluation metric. A synthesized image is counted as a correct prediction when all detected objects, whether for spatial relationships, color, or size, are accurate. For the curated COCO subset, we report  $\mathbf{AP}_{50}$  to measure the alignment of the input layout and synthesized images. Additionally, we employ **CLIP score** to evaluate the fidelity of synthesized images to textual conditions.

**Implementation Details.** Unless specified otherwise, we use the official Stable Diffusion V-1.4 [26] trained on the LAION-5B [29] dataset as the base text-to-image synthesis model. The synthesized images, with a resolution of  $512 \times 512$ , are generated with 51 denoising steps. For the hyperparameters, we use the loss scale factor  $\gamma = 30$ ,  $\alpha = 0.2$  and  $\beta = 0.8$ . Classifier-free guidance [13] is utilized with a fixed guidance scale of 7.5. Given that the layout of the synthesized image is typically established in early

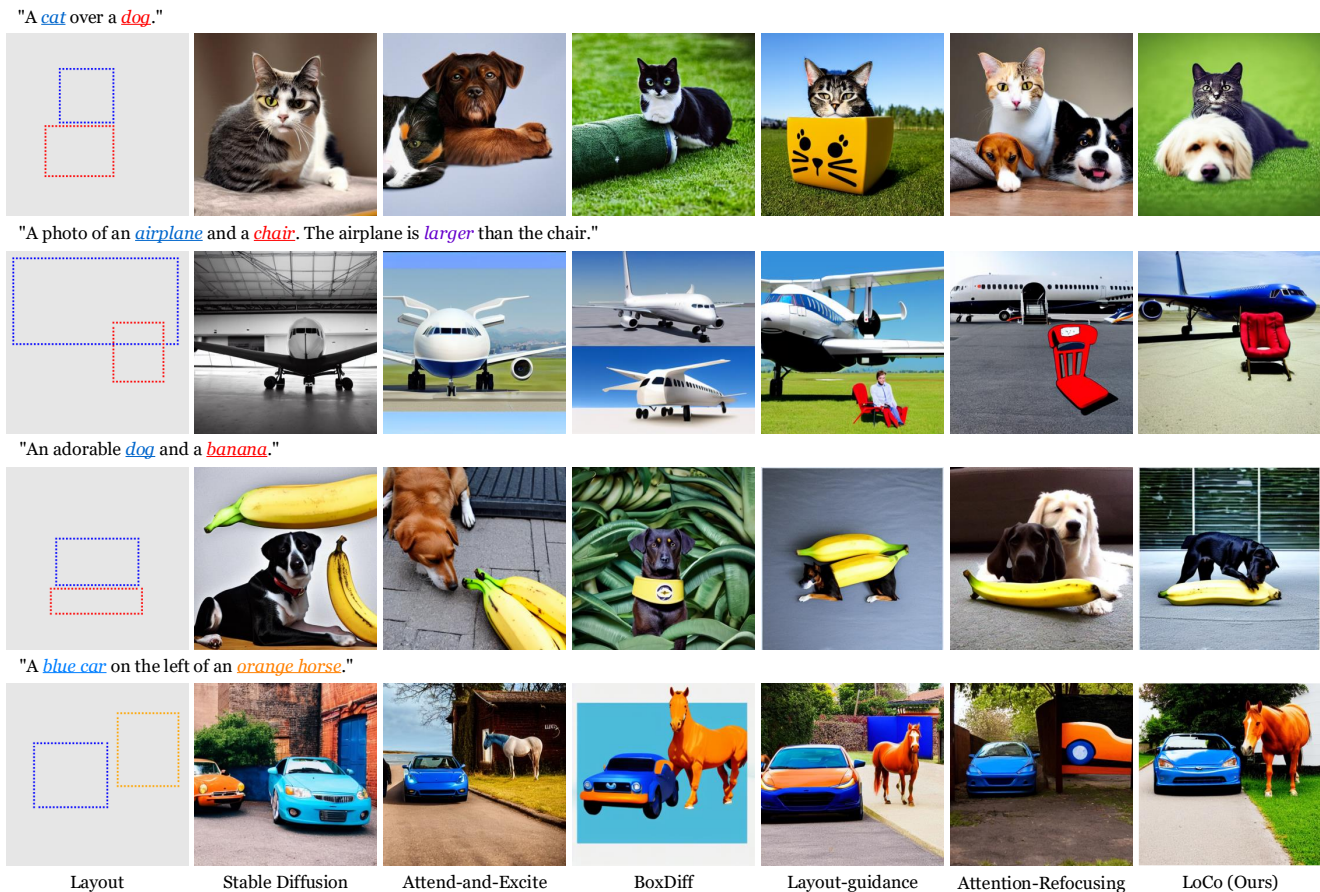


Figure 5. **Visual comparison with previous methods.** All methods take the same textual prompts and layout as inputs. Our results faithfully adhere to both textual and layout conditions, outperforming previous approaches in terms of spatial control and image quality. Please zoom in for the best view.

timesteps of inference, we integrate guidance with proposed constraints during the initial 10 steps. In each timestep, the latent update in Eq. (8) iterates 5 times before denoising.

## 4.2. Quantitative Results

Table 1. Comparison with training-free layout-to-image synthesis methods.<sup>†</sup>: A&R denotes Attention-Refocusing [21].

| Methods               | HRS-Bench    |              |              | DrawBench     | CLIP(↑)       |
|-----------------------|--------------|--------------|--------------|---------------|---------------|
|                       | Spatial(↑)   | Size(↑)      | Color(↑)     | Positional(↑) |               |
| Stable Diffusion[26]  | 10.08        | 12.05        | 13.01        | 12.50         | 0.3070        |
| Attend-and-Excite[5]  | 14.15        | 13.28        | 18.23        | 20.50         | 0.3081        |
| MultiDiffusion[4]     | 16.86        | 13.54        | 17.55        | 36.00         | 0.3096        |
| DenseDiffusion[15]    | 17.56        | 14.31        | 18.27        | 30.50         | 0.3094        |
| BoxDiff[34]           | 16.52        | 13.35        | 14.51        | 32.50         | 0.3125        |
| Layout-guidance[6]    | 22.06        | 15.83        | 15.36        | 36.50         | 0.3148        |
| A&R <sup>†</sup> [21] | 24.55        | 16.63        | 21.31        | 43.50         | 0.3140        |
| LoCo (Ours)           | <b>33.32</b> | <b>19.88</b> | <b>23.10</b> | <b>55.50</b>  | <b>0.3166</b> |

We compare LoCo with various state-of-the-art layout-to-image methods based on the Stable Diffusion V-1.4 in

Table 2. LoCo serves as a plug-and-play booster when integrated to fully-supervised layout-to-image method, *e.g.*, GLIGEN [16].

| Methods              | HRS-Bench    |              |              | DrawBench    | CLIP(↑)       |
|----------------------|--------------|--------------|--------------|--------------|---------------|
|                      | Spatial(↑)   | Size(↑)      | Color(↑)     | Spatial(↑)   |               |
| GLIGEN[16]           | 40.22        | 32.13        | 16.17        | 46.50        | 0.3167        |
| GLIGEN + A&R[21]     | 53.69        | 39.96        | 23.71        | 64.50        | 0.3198        |
| GLIGEN + LoCo (Ours) | <b>56.55</b> | <b>42.77</b> | <b>25.45</b> | <b>72.00</b> | <b>0.3222</b> |

Table 1. Our approach demonstrates remarkable accuracy improvements across all categories on the HRS-Bench compared to other state-of-the-art methods. Notably, it achieves an approximately 9% improvement over the closest competitor, Attention-Refocusing [21], in the category of spatial control. In DrawBench, LoCo also delivers a noteworthy performance improvement to the standard Stable Diffusion, showcasing its proficiency in interpreting fine-grained spatial conditions. outperforms previous approaches in image quality, as evidenced by higher CLIP scores. This suggests our approach achieves superior alignment between synthe-



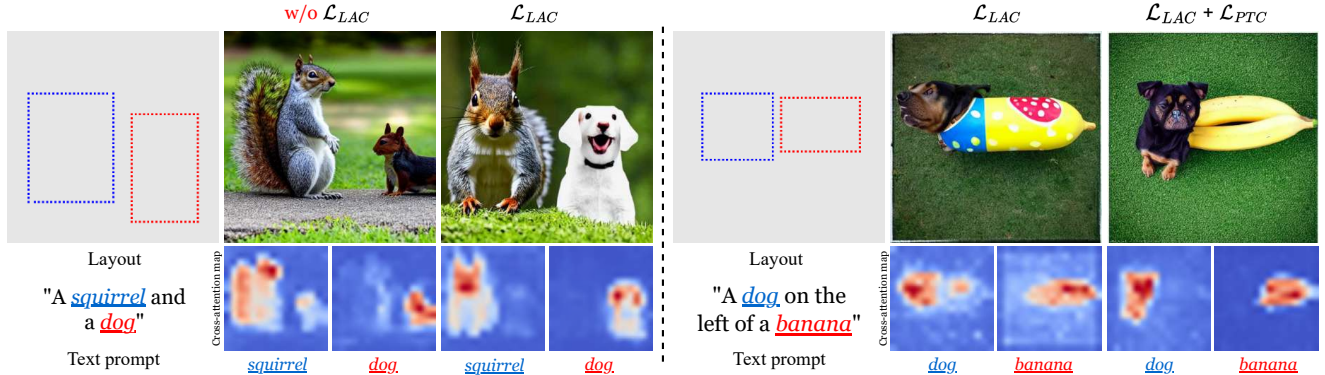


Figure 6. **Visualization of Localized Attention Constraint ( $\mathcal{L}_{LAC}$ ) and Padding Tokens Constraint ( $\mathcal{L}_{PTC}$ ).** Without  $\mathcal{L}_{LAC}$ , the high-response attention region associated with the token ”squirrel” erroneously attends to both the desired regions of ”squirrel” and ”dog”. The integration of  $\mathcal{L}_{LAC}$  effectively refines the cross-attention map, guiding it to attend precisely to the designated regions and alleviating the issue of semantic neglect. The application of  $\mathcal{L}_{PTC}$  prevents the undesired fusion of ”dog” and ”banana” when their designated locations are nearby.

sized images and textual prompts.

The integration of LoCo also significantly boosts the performance of GLIGEN [16], as depicted in Table. 2. This underscores the versatility of LoCo, serving as a plug-and-play enhancer for fully-supervised layout-to-image methods.

### 4.3. Qualitative Results

Fig. 5 provides a visual comparison of various state-of-the-art methods, illustrating that our proposed LoCo consistently facilitates the synthesis of images with more precise spatial locations, sizes, and colors.

For instance, as shown in the 1<sup>st</sup> row, given a prompt like ”A cat over a dog.” and a conditioning layout, Stable Diffusion and Attend-and-Excite fall short of generating all desired objects. BoxDiff and Layout-guidance correctly position ”cat” according to its respective box, but neglect the desired object ”dog”. Attention-Refocusing even generates two dogs. In contrast, LoCo accurately generates both the ”cat” and ”dog” based on the given layout. In the 3<sup>rd</sup> row, BoxDiff and Layout-guidance exhibit object fusion, resulting in blended ”banana” and ”dog”. Attention-Refocusing, once again, generates two dogs. Conversely, LoCo accurately generates all desired objects according to the conditioning layout while maintaining high image quality.

Moreover, we observe that LoCo implicitly encourages correct bindings between attributes and their subjects (4<sup>th</sup> row). This can be attributed to LoCo effectively mitigating the issues of object fusion and semantic neglect, thereby reducing erroneous bindings between attributes and subjects.

### 4.4. Ablation Studies

**Ablation of Key Components.** We investigate the effectiveness of critical components in our method across all cat-

Table 3. Ablation study on various combinations of components. We report performance on the HRS-Bench.

| $\mathcal{L}_{LAC}$ w/o Norm | $\mathcal{L}_{LAC}$ | $\mathcal{L}_{PTC}$ | HRS-Bench    |              |              | CLIP(↑)       |
|------------------------------|---------------------|---------------------|--------------|--------------|--------------|---------------|
|                              |                     |                     | Spatial(↑)   | Size(↑)      | Color(↑)     |               |
| ×                            | ×                   | ×                   | 10.08        | 12.05        | 13.01        | 0.3070        |
| ✓                            | ×                   | ×                   | 23.76        | 14.05        | 17.57        | 0.3124        |
| ×                            | ✓                   | ×                   | 30.24        | 18.07        | 20.16        | 0.3213        |
| ×                            | ×                   | ✓                   | 13.35        | 13.27        | 13.31        | 0.3103        |
| ✓                            | ×                   | ✓                   | 24.47        | 14.98        | 18.29        | 0.3117        |
| ×                            | ✓                   | ✓                   | <b>33.32</b> | <b>19.88</b> | <b>23.10</b> | <b>0.3166</b> |

egories in the HRS-Bench, as outlined in Table. 3. Visualized results are provided in Fig. 6.

We assess the impact of  $\mathcal{L}_{LAC}$  first.  $\mathcal{L}_{LAC}$  exhibits effectiveness even without normalization, providing competitive performance with previous state-of-the-art methods in each category. This suggests that  $\mathcal{L}_{LAC}$  is inherently advanced in controlling the spatial composition of synthesized images. However, introducing normalization in  $\mathcal{L}_{LAC}$  results in a substantial performance boost in all categories. Additionally, the synthesized images exhibit better alignment with the textual prompt, as evidenced by higher CLIP scores. This validates our crucial observation in Section 3.2 that normalization ensures a moderate guidance, avoiding semantic failures associated with over-guidance while ensuring control effects.

Moreover, solely employing  $\mathcal{L}_{PTC}$  provides a degree of spatial control (13.35%) compared to vanilla Stable Diffusion (10.08%). This underscores that padding tokens, despite lacking specific content words in the prompt, carry substantial semantic and layout information. Simultaneously utilizing  $\mathcal{L}_{LAC}$  and  $\mathcal{L}_{PTC}$  yields the best results in terms of accuracy and CLIP scores across all categories.

**Ablation on Hyperparameters.** Our approach involves

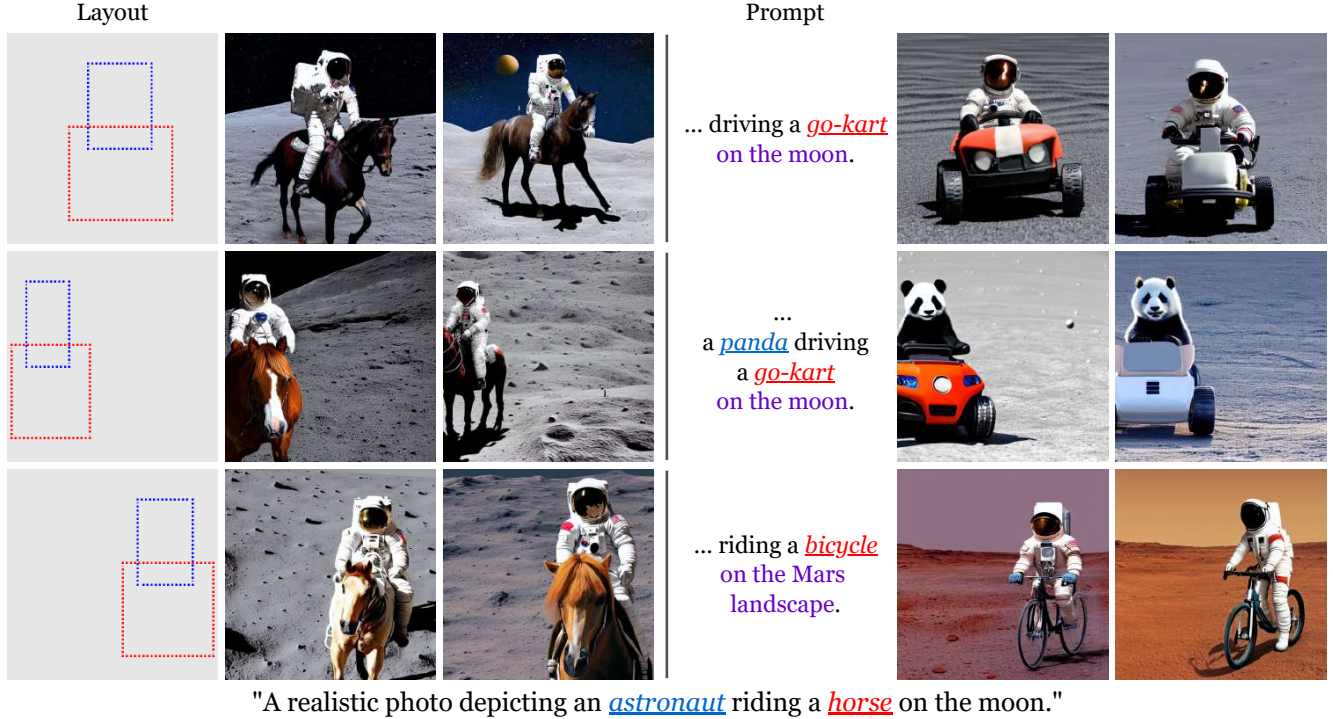


Figure 7. **Synthesized images with various conditioning inputs**, *e.g.*, different locations and desired objects. LoCo is able to handle various spatial layouts and novel scenes while maintaining high image synthesis capability and precise concept coverage.

three key hyperparameters governing LoCo’s impact: the loss scale factor  $\gamma$  for overall guidance, the guidance strength factor  $\alpha$  for  $\mathcal{L}_{PTC}$ , and the weighting factor  $\beta$  for  $\mathbf{A}_{PT}$ .

Table 4. Ablation study on loss scale  $\gamma$ . We report AP<sub>50</sub> and CLIP-Score of LoCo on the curated MS-COCO subset.

|                      | 5      | 10     | 20            | 30           | 40     | 50     | 75     | 100    |
|----------------------|--------|--------|---------------|--------------|--------|--------|--------|--------|
| AP <sub>50</sub> (↑) | 16.10  | 26.62  | 33.27         | <b>47.25</b> | 44.30  | 41.79  | 36.11  | 31.08  |
| CLIP(↑)              | 0.3005 | 0.3027 | <b>0.3042</b> | 0.3041       | 0.3005 | 0.2988 | 0.2981 | 0.2968 |

Table 5. Ablation study on various combinations of  $\alpha$  and  $\beta$ . We present performance on the *spatial* category of HRS-Bench.

| $\alpha$ | $\beta$ |       |       |       |              |       |
|----------|---------|-------|-------|-------|--------------|-------|
|          | 0       | 0.2   | 0.4   | 0.6   | 0.8          | 1.0   |
| 0        | 30.24   |       |       |       |              |       |
| 0.2      | 30.96   | 31.03 | 31.26 | 31.64 | <b>33.32</b> | 31.75 |
| 0.4      | 30.23   | 28.54 | 29.74 | 29.84 | 31.23        | 30.74 |
| 0.6      | 28.15   | 28.63 | 28.36 | 28.75 | 29.84        | 29.82 |
| 0.8      | 28.54   | 28.46 | 29.03 | 28.58 | 29.46        | 28.04 |
| 1.0      | 25.65   | 26.25 | 28.09 | 27.92 | 28.34        | 26.35 |

In Table. 4 we explore the trade-off between spatial control and image fidelity by varying  $\gamma$  from 5 to 100. Notably, as  $\gamma$  grows, both scores initially improve before experiencing a rapid decline. This phenomenon signifies that exces-

sively strong constraints significantly compromise generative fidelity, leading to a degradation in evaluation results.

With a fixed loss scale factor  $\gamma = 30$ , Table. 5 illustrates that setting  $\alpha = 0.2$  yields optimal controllability, while an increase in  $\alpha$  leads to a decline in accuracy. This also highlights the significance of maintaining mild guidance strength to synthesize high-fidelity images that align with the given layout. Although both [SoT] and [EoT] tokens contain information about the image layout, the information carried by [SoT] proves more effective in terms of layout control, as reflected in the increased accuracy with an elevated value of  $\beta$ . Therefore, employing a relatively large  $\beta$  contributes to improved performance. For  $\alpha = 0.2$ , setting  $\beta = 0.8$  achieves peak performance.

Please refer to the supplementary for additional results and ablations.

## 5. Conclusion

This paper proposes LoCo, a training-free approach for layout-to-image synthesis. We introduce two novel constraints, *i.e.*,  $\mathcal{L}_{LAC}$  and  $\mathcal{L}_{PTC}$ , which provide precise and moderate guidance in the synthesis process, mitigating semantic failures faced by previous methods and ensuring control effects. LoCo seamlessly integrates into existing text-to-image and layout-to-image models, amplifying their performance without the necessity for additional training



or paired layout-image data. Extensive experiments show case that LoCo significantly outperforms existing training-free layout-to-image approaches by a substantial margin.

## References

- [1] Omri Avrahami, Thomas Hayes, Oran Gafni, Sonal Gupta, Yaniv Taigman, Devi Parikh, Dani Lischinski, Ohad Fried, and Xi Yin. Spatext: Spatio-textual representation for controllable image generation. In *Proceedings of the IEEE/CVF Conference on Computer Vision and Pattern Recognition*, pages 18370–18380, 2023. 2, 3
- [2] Eslam Mohamed Bakr, Pengzhan Sun, Xiaogian Shen, Faizan Farooq Khan, Li Erran Li, and Mohamed Elhoseiny. Hrs-bench: Holistic, reliable and scalable benchmark for text-to-image models. In *Proceedings of the IEEE/CVF International Conference on Computer Vision*, pages 20041–20053, 2023. 5
- [3] Yogesh Balaji, Seungjun Nah, Xun Huang, Arash Vahdat, Jiaming Song, Karsten Kreis, Miika Aittala, Timo Aila, Samuli Laine, Bryan Catanzaro, et al. ediffi: Text-to-image diffusion models with an ensemble of expert denoisers. *arXiv preprint arXiv:2211.01324*, 2022. 3
- [4] Omer Bar-Tal, Lior Yariv, Yaron Lipman, and Tali Dekel. Multidiffusion: Fusing diffusion paths for controlled image generation. *arXiv preprint arXiv:2302.08113*, 2023. 6
- [5] Hila Chefer, Yuval Alaluf, Yael Vinker, Lior Wolf, and Daniel Cohen-Or. Attend-and-excite: Attention-based semantic guidance for text-to-image diffusion models. *ACM Transactions on Graphics (TOG)*, 42(4):1–10, 2023. 6
- [6] Minghao Chen, Iro Laina, and Andrea Vedaldi. Training-free layout control with cross-attention guidance. *arXiv preprint arXiv:2304.03373*, 2023. 2, 3, 4, 6
- [7] Jiaxin Cheng, Xiao Liang, Xingjian Shi, Tong He, Tianjun Xiao, and Mu Li. Layoutdiffuse: Adapting foundational diffusion models for layout-to-image generation. *arXiv preprint arXiv:2302.08908*, 2023. 2
- [8] Guillaume Couairon, Marlène Careil, Matthieu Cord, Stéphane Lathuilière, and Jakob Verbeek. Zero-shot spatial layout conditioning for text-to-image diffusion models. In *Proceedings of the IEEE/CVF International Conference on Computer Vision*, pages 2174–2183, 2023. 2, 3, 4
- [9] Weixi Feng, Xuehai He, Tsu-Jui Fu, Varun Jampani, Arjun Akula, Pradyumna Narayana, Sugato Basu, Xin Eric Wang, and William Yang Wang. Training-free structured diffusion guidance for compositional text-to-image synthesis. *arXiv preprint arXiv:2212.05032*, 2022. 3
- [10] Oran Gafni, Adam Polyak, Oron Ashual, Shelly Sheynin, Devi Parikh, and Yaniv Taigman. Make-a-scene: Scene-based text-to-image generation with human priors. In *European Conference on Computer Vision*, pages 89–106. Springer, 2022. 2
- [11] Yutong He, Ruslan Salakhutdinov, and J Zico Kolter. Localized text-to-image generation for free via cross attention control. *arXiv preprint arXiv:2306.14636*, 2023. 2, 3
- [12] Amir Hertz, Ron Mokady, Jay Tenenbaum, Kfir Aberman, Yael Pritch, and Daniel Cohen-Or. Prompt-to-prompt image editing with cross attention control. *arXiv preprint arXiv:2208.01626*, 2022. 3, 4
- [13] Jonathan Ho and Tim Salimans. Classifier-free diffusion guidance. *arXiv preprint arXiv:2207.12598*, 2022. 5
- [14] Wonjun Kang, Kevin Galim, and Hyung Il Koo. Counting guidance for high fidelity text-to-image synthesis. *arXiv preprint arXiv:2306.17567*, 2023. 3
- [15] Yunji Kim, Jiyoung Lee, Jin-Hwa Kim, Jung-Woo Ha, and Jun-Yan Zhu. Dense text-to-image generation with attention modulation. In *Proceedings of the IEEE/CVF International Conference on Computer Vision*, pages 7701–7711, 2023. 2, 3, 4, 6
- [16] Yuheng Li, Haotian Liu, Qingyang Wu, Fangzhou Mu, Jianwei Yang, Jianfeng Gao, Chunyuan Li, and Yong Jae Lee. Gligen: Open-set grounded text-to-image generation. In *Proceedings of the IEEE/CVF Conference on Computer Vision and Pattern Recognition*, pages 22511–22521, 2023. 2, 3, 6, 7
- [17] Zejian Li, Jingyu Wu, Immanuel Koh, Yongchuan Tang, and Lingyun Sun. Image synthesis from layout with locality-aware mask adaption. In *Proceedings of the IEEE/CVF International Conference on Computer Vision*, pages 13819–13828, 2021. 2
- [18] Tsung-Yi Lin, Michael Maire, Serge Belongie, James Hays, Pietro Perona, Deva Ramanan, Piotr Dollár, and C Lawrence Zitnick. Microsoft coco: Common objects in context. In *Computer Vision–ECCV 2014: 13th European Conference, Zurich, Switzerland, September 6–12, 2014, Proceedings, Part V 13*, pages 740–755. Springer, 2014. 5
- [19] Zhiheng Liu, Yifei Zhang, Yujun Shen, Kecheng Zheng, Kai Zhu, Ruili Feng, Yu Liu, Deli Zhao, Jingren Zhou, and Yang Cao. Cones 2: Customizable image synthesis with multiple subjects. *arXiv preprint arXiv:2305.19327*, 2023. 3
- [20] Wan-Duo Kurt Ma, JP Lewis, W Bastiaan Kleijn, and Thomas Leung. Directed diffusion: Direct control of object placement through attention guidance. *arXiv preprint arXiv:2302.13153*, 2023. 3
- [21] Quynh Phung, Songwei Ge, and Jia-Bin Huang. Grounded text-to-image synthesis with attention refocusing. *arXiv preprint arXiv:2306.05427*, 2023. 2, 3, 5, 6
- [22] Dustin Podell, Zion English, Kyle Lacey, Andreas Blattmann, Tim Dockhorn, Jonas Müller, Joe Penna, and Robin Rombach. Sdxl: improving latent diffusion models for high-resolution image synthesis. *arXiv preprint arXiv:2307.01952*, 2023. 3
- [23] Alec Radford, Jong Wook Kim, Chris Hallacy, Aditya Ramesh, Gabriel Goh, Sandhini Agarwal, Girish Sastry, Amanda Askell, Pamela Mishkin, Jack Clark, et al. Learning transferable visual models from natural language supervision. In *International conference on machine learning*, pages 8748–8763. PMLR, 2021. 3
- [24] Aditya Ramesh, Prafulla Dhariwal, Alex Nichol, Casey Chu, and Mark Chen. Hierarchical text-conditional image generation with clip latents. *arXiv preprint arXiv:2204.06125*, 1(2):3, 2022. 2, 3
- [25] Elad Richardson, Kfir Goldberg, Yuval Alaluf, and Daniel Cohen-Or. Conceptlab: Creative generation using diffusion prior constraints. *arXiv preprint arXiv:2308.02669*, 2023. 3

- [26] Robin Rombach, Andreas Blattmann, Dominik Lorenz, Patrick Esser, and Björn Ommer. High-resolution image synthesis with latent diffusion models. In *Proceedings of the IEEE/CVF conference on computer vision and pattern recognition*, pages 10684–10695, 2022. 2, 3, 5, 6
- [27] Olaf Ronneberger, Philipp Fischer, and Thomas Brox. U-net: Convolutional networks for biomedical image segmentation. In *Medical Image Computing and Computer-Assisted Intervention–MICCAI 2015: 18th International Conference, Munich, Germany, October 5–9, 2015, Proceedings, Part III 18*, pages 234–241. Springer, 2015. 4
- [28] Chitwan Saharia, William Chan, Saurabh Saxena, Lala Li, Jay Whang, Emily L Denton, Kamyar Ghasemipour, Raphael Gontijo Lopes, Burcu Karagol Ayan, Tim Salimans, et al. Photorealistic text-to-image diffusion models with deep language understanding. *Advances in Neural Information Processing Systems*, 35:36479–36494, 2022. 2, 5
- [29] Christoph Schuhmann, Romain Beaumont, Richard Vencu, Cade Gordon, Ross Wightman, Mehdi Cherti, Theo Coombes, Aarush Katta, Clayton Mullis, Mitchell Wortsman, et al. Laion-5b: An open large-scale dataset for training next generation image-text models. *Advances in Neural Information Processing Systems*, 35:25278–25294, 2022. 5
- [30] Wei Sun and Tianfu Wu. Learning layout and style reconfigurable gans for controllable image synthesis. *IEEE transactions on pattern analysis and machine intelligence*, 44(9): 5070–5087, 2021. 2
- [31] Zhengwentai Sun, Yanghong Zhou, Honghong He, and PY Mok. Sgdiff: A style guided diffusion model for fashion synthesis. In *Proceedings of the 31st ACM International Conference on Multimedia*, pages 8433–8442, 2023. 3
- [32] Tristan Sylvain, Pengchuan Zhang, Yoshua Bengio, R Devon Hjelm, and Shikhar Sharma. Object-centric image generation from layouts. In *Proceedings of the AAAI Conference on Artificial Intelligence*, pages 2647–2655, 2021. 2
- [33] Ruichen Wang, Zekang Chen, Chen Chen, Jian Ma, Haonan Lu, and Xiaodong Lin. Compositional text-to-image synthesis with attention map control of diffusion models. *arXiv preprint arXiv:2305.13921*, 2023. 3
- [34] Jinheng Xie, Yuexiang Li, Yawen Huang, Haozhe Liu, Wentian Zhang, Yefeng Zheng, and Mike Zheng Shou. Boxdiff: Text-to-image synthesis with training-free box-constrained diffusion. In *Proceedings of the IEEE/CVF International Conference on Computer Vision*, pages 7452–7461, 2023. 2, 3, 4, 6
- [35] Han Xue, Zhiwu Huang, Qianru Sun, Li Song, and Wenjun Zhang. Freestyle layout-to-image synthesis. In *Proceedings of the IEEE/CVF Conference on Computer Vision and Pattern Recognition*, pages 14256–14266, 2023. 3
- [36] Binbin Yang, Yi Luo, Ziliang Chen, Guangrun Wang, Xiaodan Liang, and Liang Lin. Law-diffusion: Complex scene generation by diffusion with layouts. In *Proceedings of the IEEE/CVF International Conference on Computer Vision*, pages 22669–22679, 2023.
- [37] Zhengyuan Yang, Jianfeng Wang, Zhe Gan, Linjie Li, Kevin Lin, Chenfei Wu, Nan Duan, Zicheng Liu, Ce Liu, Michael Zeng, et al. Reco: Region-controlled text-to-image generation. In *Proceedings of the IEEE/CVF Conference on Computer Vision and Pattern Recognition*, pages 14246–14255, 2023.
- [38] Yu Zeng, Zhe Lin, Jianming Zhang, Qing Liu, John Collosse, Jason Kuen, and Vishal M Patel. Scenecomposer: Any-level semantic image synthesis. In *Proceedings of the IEEE/CVF Conference on Computer Vision and Pattern Recognition*, pages 22468–22478, 2023. 2, 3
- [39] Lvmin Zhang, Anyi Rao, and Maneesh Agrawala. Adding conditional control to text-to-image diffusion models. In *Proceedings of the IEEE/CVF International Conference on Computer Vision*, pages 3836–3847, 2023. 2, 3
- [40] Bo Zhao, Lili Meng, Weidong Yin, and Leonid Sigal. Image generation from layout. In *Proceedings of the IEEE/CVF Conference on Computer Vision and Pattern Recognition*, pages 8584–8593, 2019. 2
- [41] Xingyi Zhou, Vladlen Koltun, and Philipp Krähenbühl. Simple multi-dataset detection. In *Proceedings of the IEEE/CVF Conference on Computer Vision and Pattern Recognition*, pages 7571–7580, 2022. 5